OPEN ACCESS

Kashf Journal of Multidisciplinary Research
Vol: 02 - Issue 11 (2025)
P-ISSN: 3007-1992 E-ISSN: 3007-200X
https://kjmr.com.pk

FIRST-PRINCIPLES OF ALL-INORGANIC LEAD-FREE HALIDE PEROVSKITES FOR PHOTOVOLTAIC APPLICATIONS

Tawsif Ahmad[1], Musa Khan[2], Moneeb Ahmad[3], Waqar Ahmad[4]

[1, 2, 3, 4]Department of Physics, Govt. Post Graduate College Timergara, Dir Lower, Pakistan

Affiliated with University of Malakand

[*]***Corresponding Author:*** (tawsifahamd49@gmail.com)

DOI :(*https://doi.org/10.71146/kjmr759*)

Article Info

Abstract

Lead-free inorganic halide perovskites are attractive candidates for photovoltaic and optoelectronic applications because they can combine strong light absorption with tunable electronic structures while avoiding the environmental concerns associated with Pb-containing materials. In this work, first-principles calculations are used to investigate the structural, electronic, and optical properties of cubic CsSnX3 (X = Br, I). The calculations were performed within density functional theory using the full-potential linearized augmented plane-wave approach implemented in the WIEN2k code, with the generalized-gradient-approximation PBEsol functional. Structural optimization was carried out by fitting the total-energy versus volume data with an equation-of-state approach. The calculated equilibrium structural characteristics are consistent with the reported experimental behavior, and substitution of Br by the larger I anion increases the optimized volume and lattice dimensions while reducing the bulk modulus. The calculated band structures show that the valence-band maximum and conduction-band minimum occur at the M symmetry point, indicating direct-gap semiconducting behavior. The calculated gaps are in the visible-energy range, approximately 2.1–2.3 eV, and decrease when Br is replaced by I. Total density-of-states results indicate that the valence region is dominated by Sn-s and halide-p states, whereas Sn-p, halide-p, and Cs-d states contribute strongly to the conduction region. Optical calculations further show finite static dielectric response, pronounced interbank transitions, refractive indices near 1.8 at zero photon energy, and strong absorption above the optical threshold. The results indicate that cubic CsSnX3 compounds possess electronic and optical characteristics relevant to visible-light optoelectronic and photovoltaic applications and provide a theoretical basis for further investigation of lead-free tin-halide perovskites.

Keywords: *lead-free perovskite; $CsSnX_3$; density functional theory; PBEsol; WIEN2k; band gap; dielectric function; optical absorption.*

1. Introduction

Halide perovskites with the general ABX3 composition have become important semiconductor materials for photovoltaic and optoelectronic research [1–4]. Their attractive characteristics include strong optical absorption, tunable band gaps, long carrier lifetimes and diffusion lengths, defect tolerance, and compatibility with relatively simple processing routes. These properties have supported rapid development of perovskite solar cells, light-emitting diodes, photodetectors, and related devices. The progress of lead-halide perovskites has been particularly rapid; however, the presence of lead and concerns about long-term environmental stability remain important barriers to large-scale deployment [5, 6]. Degradation under moisture, heat, light, air, and water can release lead-containing species, creating a need for alternative compositions that retain useful optoelectronic performance while reducing toxicity.

One strategy is to replace Pb2+ at the B site with chemically related actions. Group-14 elements, especially Sn2+ and Ge2+, have received substantial attention because of their charge state and chemical similarity to Pb2+. Among these alternatives, tin-based halide perovskites are especially interesting [7, 8] because they can preserve the perovskite framework and display strong optical and electronic responses. Nevertheless, Sn2+ can oxidize to Sn4+, and the resulting materials may exhibit stability challenges. Their structural and electronic behavior is therefore strongly dependent on composition, temperature, and the halide anion.

Cesium tin halides provide an all-inorganic route to lead-free perovskites. CsSnI3 can occur in orthorhombic, tetragonal, and cubic phases [8, 9] and has been associated with strong photoluminescence, p-type conductivity, and useful whole transport. CsSnBr3 also exhibits temperature-dependent structural transitions, including a cubic phase at higher temperature [9]. The halide anion affects the lattice dimensions, bonding, electronic states, and optical response because Br and I differ in ionic size and electronic structure. These effects make comparative first-principles analysis of CsSnBr3 and CsSnI3 valuable for understanding how halide substitution controls material properties.

The present study focuses on cubic CsSnX3 (X = Br, I) and examines structural, electronic, and optical characteristics using density functional theory. The objective is to determine how halide substitution affects equilibrium structural parameters, band dispersion and band-gap behavior, density of electronic states, dielectric response, refractive index, and optical absorption. Particular attention is given to the relationship between the calculated electronic structure and the optical response in the visible region. The work therefore provides a compact theoretical assessment of the suitability of these lead-free inorganic perovskites for photovoltaic and other optoelectronic applications. The choice of the cubic phase is deliberate because it provides a well-defined high-symmetry reference structure in which the effects of halide substitution can be compared directly. In real materials, CsSnI3 and CsSnBr3 can undergo temperature-dependent transitions between cubic, tetragonal, and orthorhombic structures. Structural distortions and octahedral tilting can alter the electronic states, so the calculated cubic-phase properties should be interpreted as properties of the selected structural phase rather than as a complete description of all temperature-dependent forms. This distinction is important when connecting first-principles bulk calculations with experimental device measurements.

From a materials-design perspective, the relevance of CsSnX3 is not limited to the nominal replacement of lead. The halide anion participates directly in the electronic states near the band edges, so changing Br to me can modify both the lattice and the electronic orbital overlap. The larger iodide ion expands the lattice and changes the relative energies and hybridization of Sn and halide states. Such coupled structural and electronic changes can influence the optical transition threshold, dielectric polarization, refractive response, and absorption profile. A comparative study of the two compositions therefore helps distinguish general features of the tin-halide framework from properties that are specifically controlled by the halide chemistry.

The study is also motivated by the need for theoretical screening of lead-free materials. First-principles calculations can provide a consistent way of comparing compositions before extensive experimental optimization. Structural stability, band-edge character, density of states, and optical response together offer a useful set of descriptors for judging whether a compound warrants further investigation. The present work does not claim device-level efficiency; rather, it evaluates intrinsic calculated properties that are relevant to subsequent photovoltaic and optoelectronic development.

2. Computational Methods

The calculations were performed within density functional theory (DFT), which replaces the many-electron wave function by the ground-state electron density and provides a practical framework for periodic solids. The electronic-structure calculations were carried out using the WIEN2k code and the full-potential linearized augmented plane-wave (FP-LAPW) method [17]. Exchange and correlation were treated using the generalized gradient approximation in the PBEsol form. The use of PBEsol is appropriate for obtaining reliable structural descriptions of crystalline solids and was the approach adopted in the original calculations.

The cubic CsSnX3 structures were optimized by calculating total energies for a range of cell volumes and determining the equilibrium configuration from the minimum of the energy–volume relation. The structural analysis considered the lattice volume and the associated mechanical response represented by the bulk modulus. The original study also evaluated lattice constants, bond lengths, and bond angles and compared the optimized structural parameters with available experimental values. The energy–volume curves were analyzed using an equation-of-state treatment based on the Birch–Murnaghan formulation.

After structural optimization, the electronic band structures were calculated along the high-symmetry directions of the cubic Brillouin zone. The positions of the valence-band maximum (VBM) and conduction-band minimum (CBM) were used to determine whether the materials possess direct or indirect band gaps. Total densities of states (TDOS) calculations were then used to identify the principal atomic-state contributions in the valence and conduction regions. These calculations allow the changes produced by replacing Br with me to be interpreted in terms of orbital contributions and band-edge shifts.

The optical response was evaluated from the frequency-dependent dielectric function, $\varepsilon(\omega) = \varepsilon_1(\omega) + i\varepsilon_2(\omega)$, where ε_1 and ε_2 are the real and imaginary parts, respectively. The real part provides information about polarization and dispersion, whereas the imaginary part is associated with interbank

electronic transitions and photon-energy regions where absorption is enhanced. The refractive index n (ω) and absorption coefficient α (ω) were also examined. The optical spectra were used to assess the energy range in which the materials can interact strongly with incident radiation and to relate these features to the calculated electronic band structures. In the DFT framework, the many-body problem is transformed into an effective set of single-particle Kohn–Sham equations. The central practical issue is the treatment of the exchange-correlation contribution, for which the present study adopts a generalized-gradient approximation. The PBEsol parameterization was selected in the source calculations for structural optimization and subsequent electronic and optical analysis. Unlike a simple pedagogical treatment of the Schrödinger equation, the present calculation treats the periodic crystal as an extended interacting electronic system and therefore provides the band and optical quantities required for materials characterization.

The FP-LAPW method used by WIEN2k is an all-electron approach in which the crystal potential and electronic states are treated without the pseudopotential simplification. The original work selected WIEN2k for calculations of crystalline properties and used the resulting self-consistent electronic structure to obtain the quantities reported here. Structural optimization was performed first so that the subsequent electronic and optical properties correspond to the calculated equilibrium volumes rather than arbitrary trial geometries. The resulting energy minima were then used to compare the relative structural response of the bromide and iodide systems.

For optical calculations, the frequency-dependent dielectric response was used as the central quantity from which the associated refractive and absorption behavior was interpreted. The real and imaginary components provide complementary information: ε1 describes dispersion and polarization, whereas ε2 identifies energies at which electronic transitions produce absorption. The calculated refractive index and absorption coefficient were therefore analyzed together with the band structures and TDOS rather than as isolated spectra. This combined interpretation allows the optical peaks to be linked to specific classes of electronic states.

3. Results and Discussion

3.1 Structural properties

The optimized crystal structures are based on the cubic ABX3 framework, with Cs occupying the A site, Sn occupying the B site, and Br or I occupying the halide site. The Sn2+ action is coordinated by six halide anions, forming the characteristic corner-sharing octahedral network of the perovskite structure. Figure 1 shows the calculated unit-cell representation. The structural environment changes when Br is replaced by me because the iodide anion has a larger atomic size. This substitution produces an increase in the optimized cell volume and lattice dimensions. The calculated bulk modulus decreases from the Br-containing compound to the I-containing compound, indicating a softer lattice for the iodide composition [8, 9].

The total-energy versus volume curves in Figure 2 display well-defined minima for both compositions, supporting the stability of the optimized cubic structures within the adopted computational model. The calculated structural parameters obtained with PBEsol were reported to be in good agreement with experimental values. The systematic volume increase on going from Br to me is physically consistent

with the larger size of me and demonstrates that the halide site provides a direct means of controlling the lattice dimensions. The calculated trends also show that structural modification at the anion site is accompanied by changes in the electronic and optical properties discussed below.

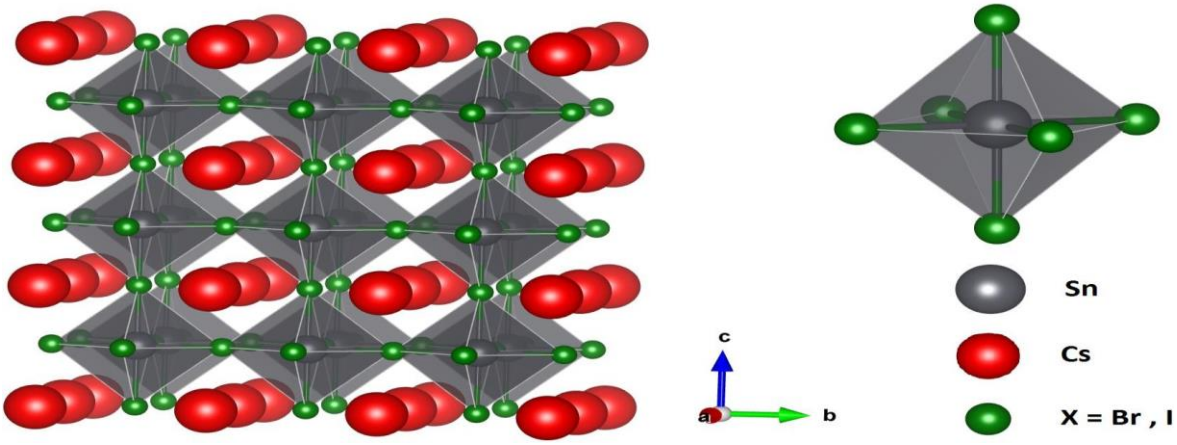

Figure 1. Cubic unit-cell structure of $CsSnX_3$ (X = Br, I), reproduced from the source study.

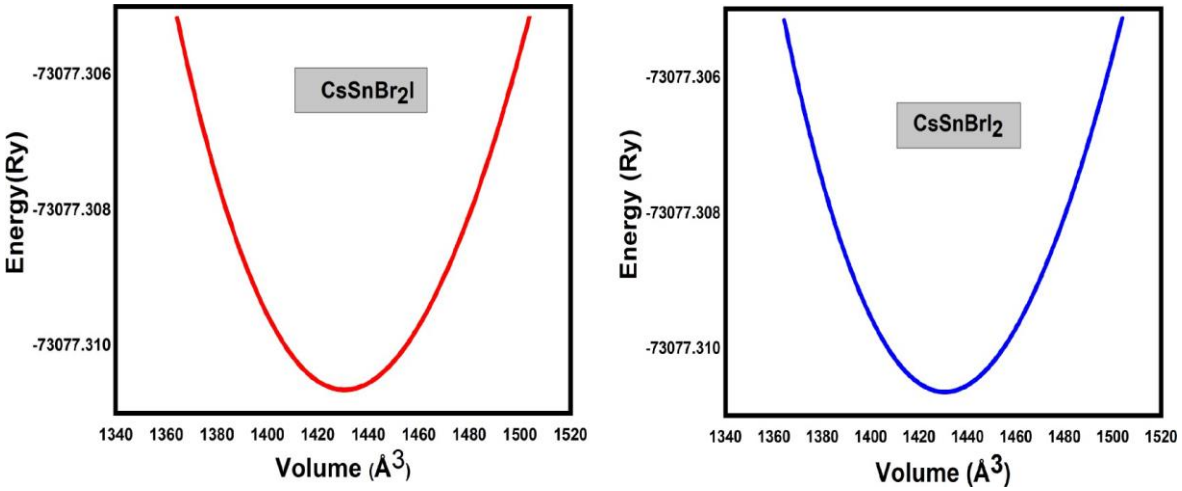

Figure 2. Ground-state energy versus optimized volume for the cubic $CsSnX_3$ structures (X = Br, I), reproduced from the source study.

3.2 Electronic structure and band gap

The calculated band structures are presented in Figure 3. For both cubic compounds, the VBM and CBM occur at the M symmetry point. The coincidence of these band extrema identifies the materials as direct-gap semiconductors within the present calculations. Direct band-gap behavior is particularly relevant to optical applications because radiative transitions can occur without requiring a momentum-changing phonon.

The calculated band gaps fall within the visible-energy range, with values reported in the approximately 2.1–2.3 eV interval. An important compositional trend is the reduction of the band gap when Br is replaced by me. The larger iodide anion changes the lattice dimensions and modifies the orbital interactions involving Cs-d, Sn-p, and halide-p states. These changes reduce the separation between the

relevant bonding and antibonding states and shift the band edges toward one another. Consequently, halide substitution provides a route for tuning the electronic gap while preserving the basic cubic perovskite framework.

The visible-range band gaps are significant for photovoltaic and optoelectronic applications because they allow the materials to interact with a substantial portion of the incident solar spectrum. At the same time, the calculated gaps are sufficiently large to place the principal absorption threshold in the visible region. The results therefore suggest that the two compositions can serve as useful model systems for studying the relationship between halide chemistry, electronic structure, and optical response in lead-free perovskites.

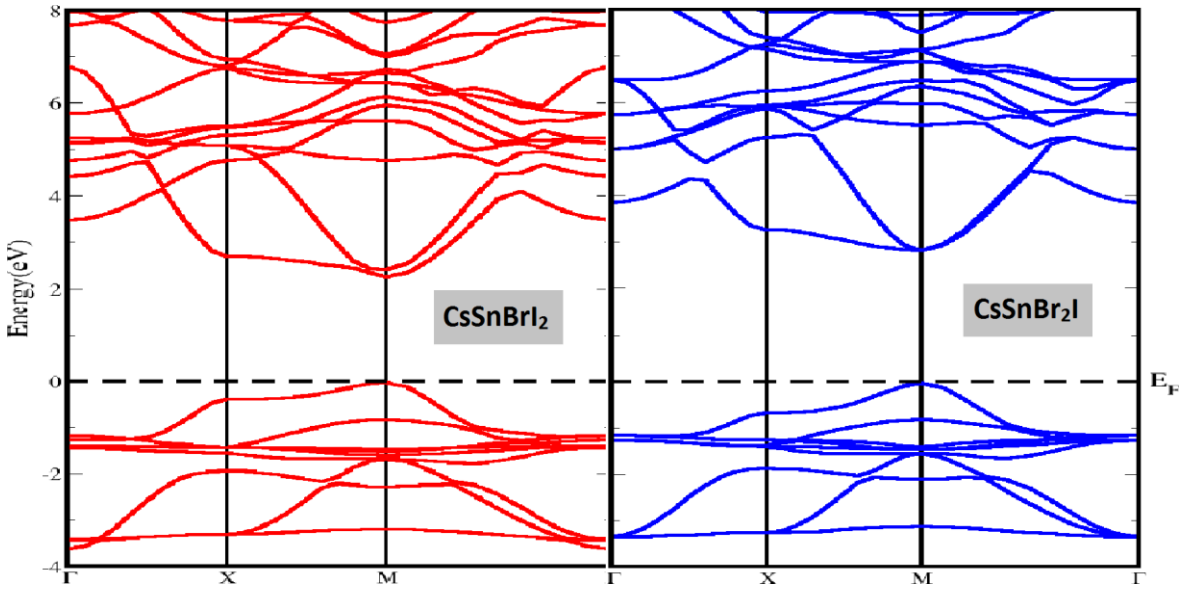

Figure 3. Electronic band structures of cubic $CsSnX_3$ (X = Br, I), reproduced from the source study.

3.3 Density of states and bonding

The total density of states in Figure 4 provides additional information about the origin of the calculated bands. The valence region contains major contributions from Sn-s and halide-p states, with Cs-p states also contributing. In the conduction region, the principal contributions arise from Sn-p, halide-p, and Cs-d states. For the bromide-containing system, the source analysis identifies Sn-s and Br-p states as important contributors between approximately −3 and 0 eV, while Sn-p and Br-p states contribute strongly in the conduction region around 2.3–5.5 eV. The corresponding iodide states modify the distribution of electronic states and contribute to the reduction of the band gap.

The density-of-states results are consistent with the band-structure analysis and help explain the optical transitions. The interaction between Sn and the halide ions has a substantial covalent component associated with orbital hybridization, while the Cs–halide interaction has a stronger ionic character. The calculated charge-density analysis in the original study indicated covalent connections between Sn and the halide ions on the (110) plane and ionic interactions between Cs and halide ions on the (100) plane.

These bonding characteristics provide a microscopic basis for the observed sensitivity of the electronic structure to halide substitution.

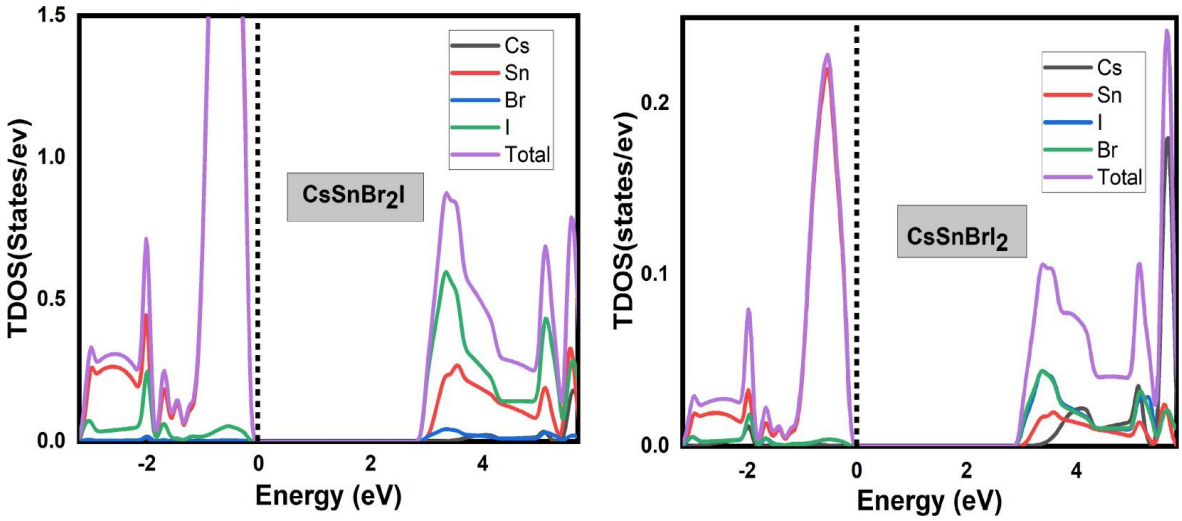

Figure 4. Total density of states of cubic $CsSnX_3$ (X = Br, I), reproduced from the source study.

3.4 Optical properties

The calculated dielectric functions are shown in Figures 5 and 6. The real part, ε1 (ω), represents the dispersive and polarizable response of the material. The reported zero-energy value is approximately 3.2 for the cubic CsSnX3 phases. The real dielectric function increases at low photon energies, reaches pronounced maxima, and becomes negative in the higher-energy region, approximately 18–22 eV. Negative ε1 values are associated with strong reflection and attenuation of electromagnetic radiation in that energy ranges [19].

The imaginary part, ε2 (ω), describes the absorptive component of the dielectric response and provides direct information about allowed interbank transitions. The calculated spectra show critical features beginning around 2.3 eV, consistent with the calculated optical band gaps. These features arise from transitions between valence-band states containing Sn-s and halide-p character and conduction-band states dominated by Sn-p, halide-p, and Cs-d character. Additional peaks occur at higher photon energies, extending approximately from 3.4–4.5 eV to about 20 eV, reflecting transitions involving deeper valence states and higher conduction states.

The refractive-index spectra in Figure 7 provide another measure of the optical response. The calculated zero-frequency refractive index is approximately 1.8 for the cubic compounds. The spectra show additional structures at higher energies, extending from the visible toward ultraviolet and far-ultraviolet regions. The variation of refractive index with photon energy reflects the corresponding frequency dependence of the dielectric response. The reported reduction of the refractive index below unity at selected higher-energy regions is associated in the source analysis with dispersive behavior and energy dissipation.

The absorption coefficient spectra in Figure 8 show negligible absorption below the principal optical threshold followed by a strong increase in the visible/near-visible energy region. The calculated

absorption becomes pronounced above approximately 2.2–2.3 eV and displays multiple high-energy peaks. The absorption features are consistent with the interbank transitions identified from the imaginary dielectric function. Such strong absorption above the band edge is desirable for thin optically active layers because efficient photon absorption can be achieved over a relatively short propagation distance.

Taken together, the optical results show that CsSnBr3 and CsSnI3 possess substantial dielectric response, finite refractive indices, and strong absorption in energy ranges relevant to visible-light optoelectronics. The reduction in band gap produced by replacing Br with I is accompanied by changes in the dielectric and refractive responses. Thus, halide selection is not only a structural parameter but also an effective means of tuning the optical behavior of the perovskite lattice.

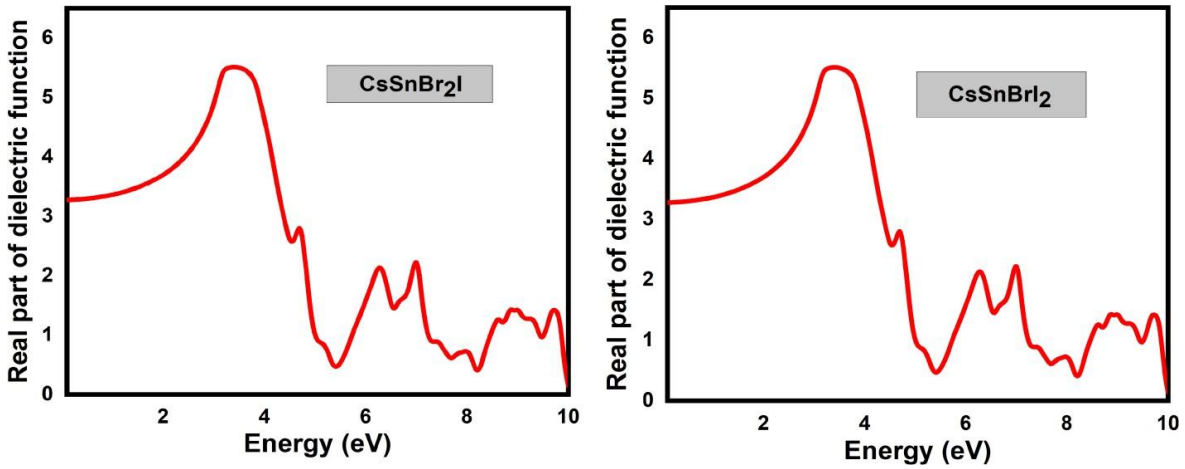

Figure 5. Real part of the dielectric function $\varepsilon_1(\omega)$ for cubic $CsSnX_3$ (X = Br, I), reproduced from the source study.

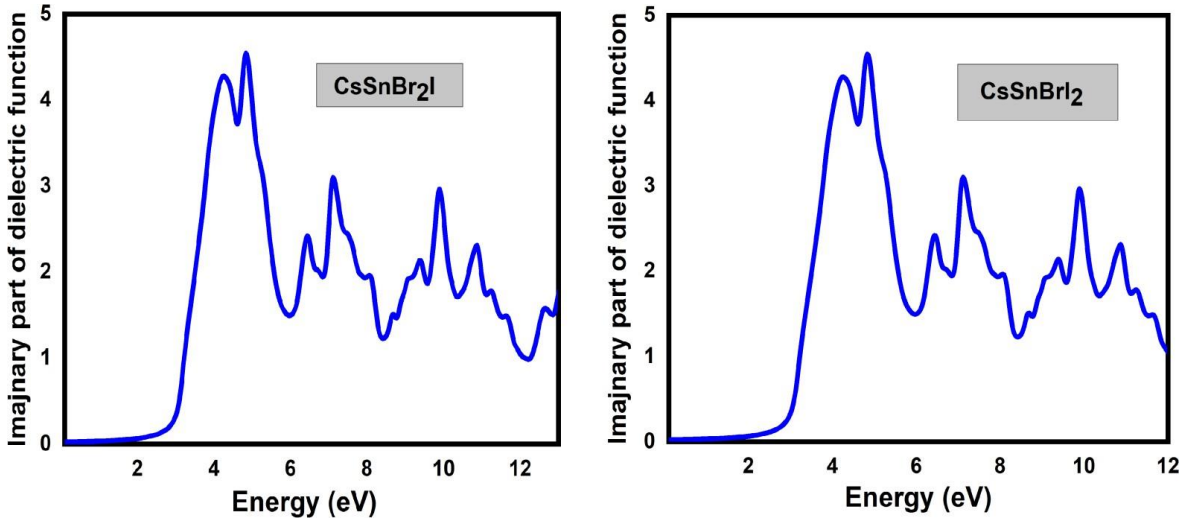

Figure 6. Imaginary part of the dielectric function $\varepsilon_2(\omega)$ for cubic $CsSnX_3$ (X = Br, I), reproduced from the source study.

The structural and electronic results demonstrate that the effects of halide substitution are coupled. Figure 1 illustrates the three-dimensional framework of corner-sharing SnX6 octahedra, with Cs ions occupying the larger cavities. The Sn-centered octahedral environment is particularly important because the Sn and halide orbitals contribute substantially to the states around the band edges. When the halide is

changed from Br to me, the larger ionic size produces a larger equilibrium volume. The corresponding reduction in bulk modulus indicates that the I-containing lattice is more compressible within the calculated cubic structure. These trends are useful indicators of how chemical substitution changes the mechanical environment in which electronic states develop.

Figure 2 provides an energetic view of the same structural response. Each composition has a minimum in the calculated total-energy curve, allowing an equilibrium volume to be identified. The smooth parabolic-like shape around the minimum is consistent with a stable equilibrium configuration. The shift in the minimum between the two compositions is a direct manifestation of the larger iodide anion. The structural changes are not merely geometric: they alter interatomic distances and therefore modify the orbital overlap responsible for the band-edge states.

Figure 3 shows that the band extrema remain at the same high-symmetry point for both compositions even though the energy separation changes. This indicates that halide substitution tunes the magnitude of the band gap without changing the direct nature of the fundamental transition in the calculated cubic structures. Such retention of the direct-gap character is important because it means that the substitution can alter the spectral position of the absorption edge without introducing a momentum mismatch between the valence and conduction extrema.

The reduction of the band gap from Br to me can be understood from the combined effect of increased lattice dimensions and changed orbital interactions. The source analysis associates the shift with modified coupling among Cs-d, Sn-p, and halide-p states and a reduction in the separation of bonding and antibonding levels. The larger, more polarizable iodide ion therefore changes both the local chemical environment and the distribution of states near the Fermi level. This provides a consistent explanation for the red-shift of the optical response expected from the smaller calculated gap.

The TDOS in Figure 4 complements the band structures by showing where the available electronic states are concentrated. The finite density of states on both sides of the band gap is separated by a clear low-density region associated with the semiconducting gap. In the valence region, Sn-s and halide-p contributions are prominent, while the conduction region contains substantial Sn-p, halide-p, and Cs-d character. Because the same classes of states occur in the dielectric-function transitions, the TDOS provides a direct qualitative bridge between the calculated electronic structure and optical spectra.

The reported bonding analysis further indicates that Sn–halide interactions are primarily covalent, whereas Cs–halide interactions are predominantly ionic. Covalent Sn–X bonding is associated with orbital hybridization and therefore strongly influences the electronic states close to the band edges. In contrast, the more ionic Cs–X interaction helps stabilize the crystal framework and contributes to the electrostatic environment experienced by the SnX_6 network. The coexistence of these bonding characteristics is a typical feature of complex inorganic perovskite structures and helps explain why changes at the halide site can propagate through the electronic structure.

The real dielectric response in Figure 5 starts from a finite low-energy value and exhibits strong dispersion as photon energy increases. The reported $\varepsilon_1(0)$ of approximately 3.2 indicates a measurable electronic polarizability in the static limit. The prominent maxima at low photon energies are consistent

with the proximity of strong interbank transitions. At higher energy, the real part crosses toward negative values, reaching negative regions around 18–22 eV. In such regions, the electromagnetic response becomes strongly dispersive and reflective, which is relevant when considering the material response beyond the solar spectrum.

Figure 6 shows the imaginary dielectric component, where the onset of substantial response occurs near the calculated optical gap. The first important features around 2.3 eV correspond to transitions across the fundamental gap. Additional structures at higher energies reflect transitions from deeper valence states into higher conduction states. The calculated spectra thus contain information extending well beyond the first absorption edge. This broad energy response is consistent with the multi-orbital electronic structure observed in the TDOS.

The refractive-index curves in Figure 7 follow the expected connection with the dielectric response. A zero-energy value of approximately 1.8 indicates a moderate optical density at low photon energy. The strong energy dependence demonstrates that the refractive response cannot be represented adequately by a single constant across the full spectrum. Features in the visible region are followed by additional structures in the ultraviolet and far-ultraviolet ranges. The source analysis also notes regions where the calculated refractive index falls below unity; these should be interpreted as highly dispersive spectral regions rather than as evidence that ordinary information or energy propagation universally exceeds its vacuum counterpart.

The absorption coefficient in Figure 8 provides the most direct indication of the spectral range in which the materials can efficiently attenuate incident light. The absorption rises sharply near the fundamental optical threshold and develops several pronounced peaks at higher photon energies. The reported peaks extending through approximately 4.5–20 eV are consistent with the sequence of interbank transitions identified in $\varepsilon 2(\omega)$. Strong absorption in the visible range is favorable for photovoltaic absorber layers, although actual device performance also depends on carrier mobility, recombination, defects, interfaces, film morphology, phase stability, and electrode properties, none of which were evaluated in the present bulk calculations.

An important outcome of the optical analysis is that the Br-to-I substitution changes the optical response in the same direction as the electronic band-gap change. A narrower gap moves the onset of electronic transitions toward lower photon energy, while changes in lattice dimensions and orbital hybridization alter the magnitude and position of subsequent spectral features. Thus, the structural, electronic, and optical results are internally consistent: the chemical change at the halide site modifies the lattice, the lattice modifies orbital interactions, and those interactions determine the band edges and frequency-dependent optical response.

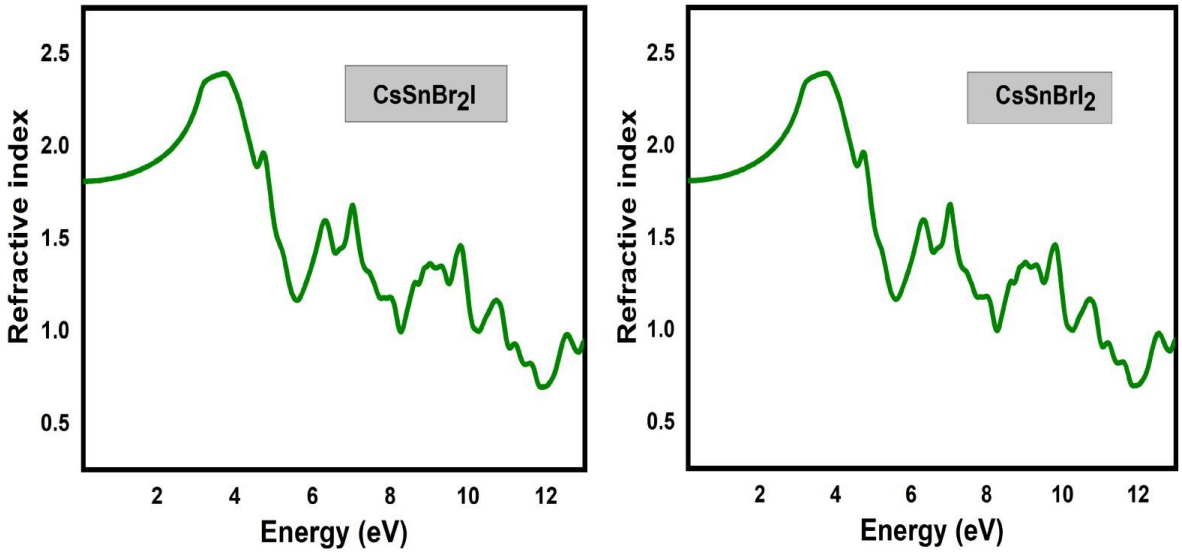

Figure 7. Refractive index n (ω) of cubic $CsSnX_3$ (X = Br, I), reproduced from the source study.

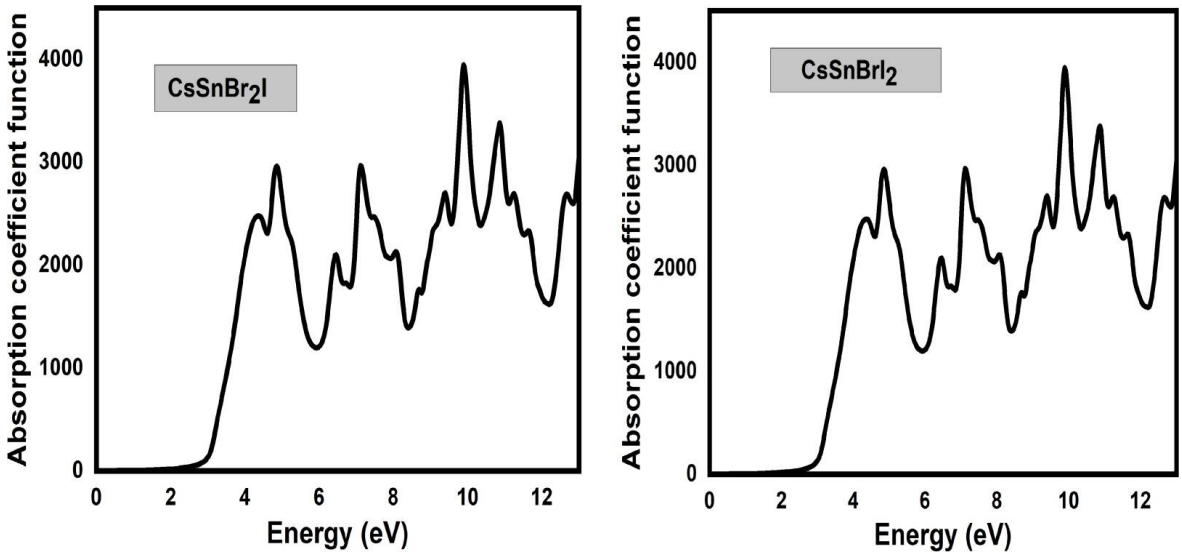

Figure 8. Absorption coefficient α (ω) of cubic $CsSnX_3$ (X = Br, I), reproduced from the source study.

4. Conclusion

This first-principles investigation examined the structural, electronic, and optical properties of cubic lead-free CsSnX3 (X = Br, I) halide perovskites using the FP-LAPW method implemented in WIEN2k and the PBEsol generalized-gradient approximation. The optimized energy–volume curves support stable cubic configurations within the computational model, while substitution of Br by the larger I anion increases the lattice volume and decreases the bulk modulus. The calculated structural trends are consistent with the reported experimental behavior.

Both compounds exhibit direct band gaps because the VBM and CBM are located at the M symmetry point. Their calculated band gaps lie in the visible region, approximately 2.1–2.3 eV, and the gap narrows when Br is replaced by me. The TDOS analysis shows that Sn-s and halide-p states dominate

important portions of the valence band, whereas Sn-p, halide-p, and Cs-d states contribute strongly to the conduction region. The bonding analysis indicates a predominantly covalent interaction between Sn and the halide ions and a more ionic interaction between Cs and the halides.

The optical calculations further demonstrate a static real dielectric response of about 3.2 and a zero-frequency refractive index near 1.8, together with strong interbank transitions beginning around 2.2–2.3 eV. The absorption spectra show strong absorption above the optical threshold, while additional dielectric, refractive, and absorption features extend into the ultraviolet region. Overall, the calculated properties support the potential of cubic $CsSnX_3$ compounds as lead-free materials for visible-light photovoltaic and optoelectronic applications. Further experimental work should evaluate phase stability, oxidation behavior, film quality, and device performance to determine how closely these idealized bulk properties can be translated into practical devices.

References

1. Kojima A, Teshima K, Shirai Y, Miyasaka T. Organometal halide perovskites as visible-light sensitizers for photovoltaic cells. J Am Chem Soc. 2009;131:6050–6051.
2. Jena AK, Kulkarni A, Miyasaka T. Halide Perovskite Photovoltaics: Background, Status, and Future Prospects. Chem Rev. 2019;119:3036–3103.
3. Manser JS, Christians JA, Kamat PV. Intriguing Optoelectronic Properties of Metal Halide Perovskites. Chem Rev. 2016;116:12956–13008.
4. Chouhan L, Ghimire S, Subrahmanyam C, Miyasaka T, Biju V. Synthesis, optoelectronic properties and applications of halide perovskites. Chem Soc Rev. 2020;49:2869–2905.
5. Babayigit A, Ethirajan A, Muller M, Conings B. Toxicity of organometal halide perovskite solar cells. Nat Mater. 2016;15:247–251.
6. Hoefler SF, Trimmel G, Rath T. Progress on lead-free metal halide perovskites for photovoltaic applications: a review. Monatsh Chem. 2017;148:795–826.
7. Goldschmidt VM. Die Gesetze der Krystallochemie. Naturwissenschaften. 1926;14:477–485.
8. Weber D. CH3NH3SnBrxI3−x (x = 0–3), ein Sn(II)-System mit kubischer Perowskitstruktur. Z Naturforsch B. 1978.
9. Møller CK. A phase transition in cæsium plumbochloride. Nature. 1957;180:981–982; and related crystal-structure studies of cesium lead halides. Nature. 1958;182:1436.
10. Chung I, Lee B, He J, Chang RPH, Kanatzidis MG. All-solid-state dye-sensitized solar cells with high efficiency. Nature. 2012;485:486–489.
11. Jones RO, Gunnarsson O. The density functional formalism, its applications and prospects. Rev Mod Phys. 1989;61:689–746.
12. Born M, Oppenheimer R. Zur Quantentheorie der Molekeln. Ann Phys. 1927;389:457–484.
13. Hohenberg P, Kohn W. Inhomogeneous electron gas. Phys Rev. 1964;136:B864–B871.
14. Dreizler RM, Gross EKU. Density Functional Theory: An Approach to the Quantum Many-Body Problem. Springer; 1990.
15. Perdew JP, Burke K, Ernzerhof M. Generalized gradient approximation made simple. Phys Rev Lett. 1996;77:3865–3868.
16. Lejaeghere K, Bihlmayer G, Björkman T, et al. Reproducibility in density-functional theory calculations of solids. Science. 2016;351:aad3000.
17. Blaha P, Schwarz K, Madsen GKH, Kvasnicka D, Luitz J. WIEN2k: An Augmented Plane Wave + Local Orbitals Program for Calculating Crystal Properties. Vienna University of Technology; 2001.
18. Birch F. Finite elastic strain of cubic crystals. Phys Rev. 1947;71:809–824.
19. Penn DR. Wave-number-dependent dielectric function of semiconductors. Phys Rev. 1962;128:2093–2097.
20. Murtaza G, Ahmad I, Amin B, Afaq A, Maqbool M, Maqsood J, Khan I, Zahid M. Optical properties of halide perovskite compounds. Opt Mater. 2011;33:553–557.